Article

Designing Actuation Concepts for Adaptive Slabs with Integrated Fluidic Actuators Using Influence Matrices

Markus Nitzlader [1,*], Simon Steffen [1], Matthias J. Bosch [2], Hansgeorg Binz [2], Matthias Kreimeyer [2] and Lucio Blandini [1]

1   Institute for Lightweight Structures and Conceptual Design (ILEK), University of Stuttgart, Pfaffenwaldring 14, 70569 Stuttgart, Germany
2   Institute for Engineering Design and Industrial Design (IKTD), University of Stuttgart, Pfaffenwaldring 9, 70569 Stuttgart, Germany
*   Correspondence: markus.nitzlader@ilek.uni-stuttgart.de

Abstract: Previous work has shown that floor slabs make up most of the material mass of building structures and are typically made of reinforced concrete. Considering the associated resource consumption and greenhouse gas emissions, new approaches are needed in order to reduce the built environment's impact on the ongoing climate crisis. Various studies have demonstrated that adaptive building structures offer a potential solution for reducing material resource consumption and associated emissions. Adaptive structures have the ability to improve load-bearing performance by specifically reacting to external loads. This work applies the concept of adaptive structures to reinforced concrete slabs through the integration of fluidic actuators into the cross-section. The optimal integration of actuators in reinforced concrete slabs is a challenging interdisciplinary design problem that involves many parameters. In this work, actuation influence matrices are extended to slabs and used as an analysis and evaluation tool for deriving actuation concepts for adaptive slabs with integrated fluidic actuators. To define requirements for the actuator concept, a new procedure for the selection of actuation modes, actuator placement and the computation of actuation forces is developed. This method can also be employed to compute the required number of active elements for a given load case. The new method is highlighted in a case study of a 2 m × 2 m floor.

Keywords: adaptive structures; slabs; integrated actuators; influence matrices; actuator placement; multi-axial load transfer

1. Introduction

1.1. Previous Work

The construction industry is responsible for around 60% of global resource consumption, 50% of global waste generation, approximately 40% to 50% of global emissions of greenhouse gases and more than 35% of global energy consumption [1,2]. Identifying potential savings and thus reducing resource consumption, energy expenditure and emissions is essential for the sustainable development of our built environment.

Previous analyses based on [3–5] have shown that floor slabs in building structures contribute significantly to the total mass. Reinforced concrete slabs are one of the most widespread components due to the low cost and ease of construction [6]. Reinforced concrete construction involves high process-related greenhouse gas emissions, which is a cause of concern for the ongoing climate crisis. In addition, concrete structures require considerable amounts of sand, which is becoming increasingly scarce [7,8]. The load transfer in floor slabs takes place primarily through bending. Usually, this means that serviceability limit states, mostly deflection limits, are the governing criteria for sizing [9]. For example, it may be necessary to increase the thickness of a slab in order to limit bending-induced deformations and thus prevent damage to adjacent structural and non-structural elements. Optimisation strategies for passive reinforced concrete slabs quickly lead to a shift in the

dead weight to live load ratio [10] increasing the significance of the variable live loads. The design load almost never occurs during the service time of the structure, so a large part of the material remains unused most of the time. In addition to this, conventional strategies such as pre-cambering can only be implemented for permanent loads [9].

Structural adaptation to loading through integrated actuators offers a potential solution for reducing material resource consumption and associated greenhouse gas emissions [11–13]. Early investigations into the manipulation of stress, deformations and vibrations in civil engineering structures were carried out in the 1970s [14–16]. Structural adaption requires sensors, actuators and a control unit. Through sensors, the state of a structure is monitored and the deviation from the desired state can be calculated. Actuators can then be employed to manipulate the structural behaviour, for example by reducing the displacements until the desired state is reached. One possible way is to replace a column in a truss structure with a hydraulic jack. When the hydraulic jack extends, the structure deforms. Well-designed adaptive structures can react to external stimuli in such a way that the stress is homogenised [17], deformations are reduced [18–20] or vibrations are damped [17,20,21]. For stiffness-governed designs, the ability to manipulate deflections results in significant potential savings in materials and emissions [22–25].

The design of adaptive structures has been carried out using various methods based on optimisation formulations and sensitivity analyses [21,24,26–28]. The work in [17,29–31] focuses on 2-dimensional thin-walled structures including shear walls, plates and shells. Here, the optimisation task for the actuator placement as well as the computation of the actuation forces was done on the basis of Computer Aided Geometric Design with sensitivity matrices, heuristic approximation methods, such as simulated annealing or evolutionary algorithms, and an optimisation based on the Gramian compensability matrix.

The method of influence lines and surfaces makes it possible to analyse and evaluate the load-bearing behaviour of structures for different load positions [32,33]. Similar to the idea of this method, actuation influence matrices quantify the effect on the structural response (e.g., forces and deformations) caused by a unit load applied through a single actuator or, in a more abstract form, a single active element. A general form of this discrete method is derived in [34] for truss and beam structures. Actuation influence matrices have been employed to obtain optimal actuator placements as well as to compute actuation forces for a desired structural state [34,35].

In the context of the Collaborative Research Centre (SFB) 1244 "Adaptive Skins and Structures for the Built Environment of Tomorrow" at the University of Stuttgart, fluidic actuators are integrated into the cross-section of beams and slabs which are subjected to bending. This way of integrating actuators takes a different approach, as adaptive structures usually have externally added actuators or are composed of truss structures in which single bars are actuated. A fluidic actuator can be a hydraulic pressure chamber placed in the compression zone at a certain distance to the neutral axis. When hydraulic pressure is provided, it causes the chambers to expand, thus producing a bending moment that counteracts the bending moment caused by the external load. This reduces deflections and critical tensile stresses. An example of such an actuator is the fluidic actuator used in [18,22], shown in Figure 1. It is a lens-shaped pressure chamber made of two welded steel sheets.
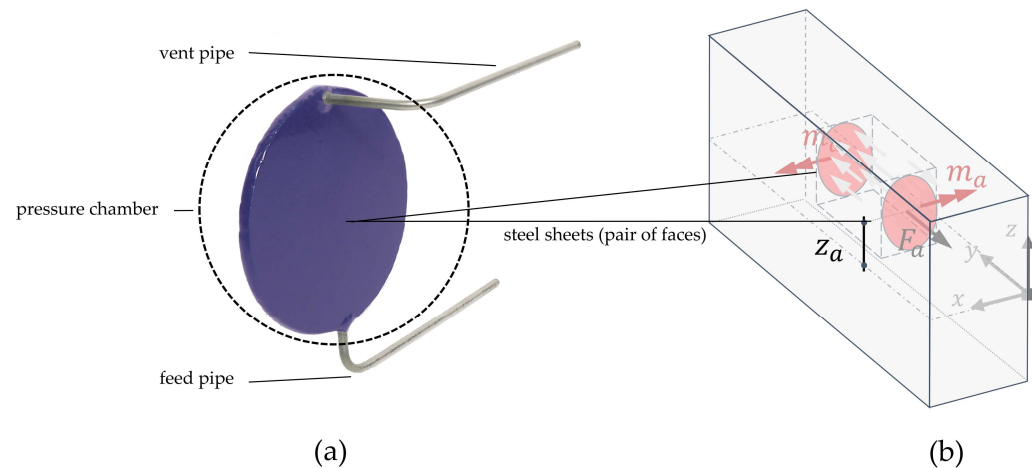
Figure 1. (**a**): Fluidic actuator used in [18] for a beam; (**b**): representation of the actuation faces (pair of faces) which are pushed apart by hydraulic pressure.

The opposing steel sheets (pair of faces) are pushed apart by hydraulic pressure. Numerical and experimental investigations of integrated fluidic actuators in reinforced concrete beams have shown potential for the manipulation of deformations [18,22,36,37].

1.2. New Contribution

The generation of forces and strokes with the use of auxiliary energy can be achieved through a variety of functional principles. Divided into sub-functions, an actuator consists of an energy converter, a conductor and supplier [38,39]. The actuator concept is understood as the ideal combination of these three sub-functions.

In two-way slabs, bending moments from external loads do not just occur in the x-direction. The actuation concept of integrated fluidic actuators presented for uniaxial load transfer must therefore be extended to multi-axial load transfer. For this purpose, face pairs in several spatial directions above the neutral plane are considered. Pushing these face pairs apart through actuation induces moments in the *x*, *y* and *xy* directions. The actuation concept is influenced by different design parameters such as the control objective, the actuation modes, the adaptation level, the actuator placement and the computation of the required actuation forces.

The design of an adaptive structure is a multi-disciplinary and iterative process in which various factors have to be taken into account. In this work, actuation concepts are not developed as usual by employing stock actuators. The following method can be used to create a list of requirements for the actuator concept. Conversely, the method also allows the requirements of the actuator concept to be taken into account. An optimal adaptive structure, in terms of material and emission efficiency, can be achieved using such an integrated approach whereby the actuation and actuator concept are harmonised with each other.

This work builds on and extends the methods developed in [22] for the integration of fluidic actuators in reinforced concrete structures and [34] concerning the use of actuation influence matrices for the design of the actuation concepts respectively of the individual design parameters. New contributions offered by this work are:

1. The elaboration of a new actuation concept based on fluidic actuators that can be integrated into floor slabs to control the response under loading.
2. Extension of actuation influence matrices to two-way slabs.
3. Computation of actuation forces and design spaces for actuator placement based on influence matrices.
4. A new methodology that makes it possible to co-design actuation and actuator concepts for adaptive floor slabs.

2. Materials and Methods

2.1. Influence Matrices

The model adopted for plate structures is based on Reissner–Mindlin Plate Theory with bilinear shape functions on a quadrilateral element with 4 corner nodes and 4 Gauss nodes as shown in Figure 2 and [40–42].

(a)   (b)
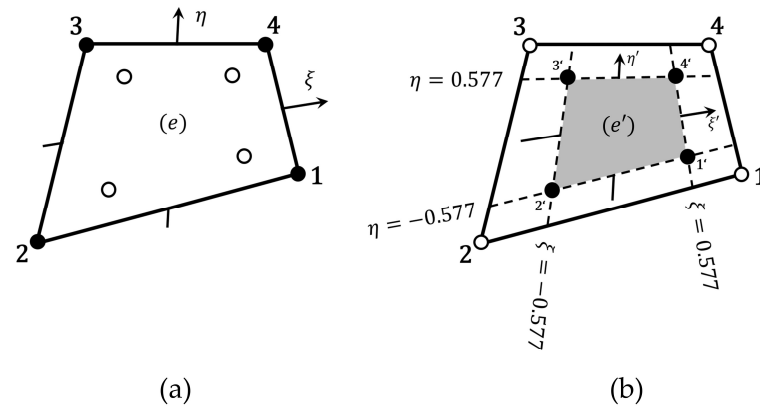
Figure 2. (**a**)*:* Element (e) with corner nodes 1–4 and (**b**)*:* gauss Element (e′) with gauss nodes 1′–4′.

Therefore, the element stiffness matrix has 12 by 12 entries. The order of the entries of the element deformation $d^{(e)}$ and force $f^{(e)}$ vectors are as follows:

$$d^{(e)} = \begin{bmatrix} w_1 & \varphi_{x1} & \varphi_{y1} & w_2 & \varphi_{x2} & \varphi_{y2} & w_3 & \varphi_{x3} & \varphi_{y3} & w_4 & \varphi_{x4} & \varphi_{y4} \end{bmatrix}^T \tag{1}$$

$$f^{(e)} = \begin{bmatrix} F_{z1} & M_{x1} & M_{y1} & F_{z2} & M_{x2} & M_{y2} & F_{z3} & M_{x3} & M_{y3} & F_{z4} & M_{x4} & M_{y4} \end{bmatrix}^T \tag{2}$$

Assuming a slab with *DOF* degrees of freedom and $i^{\#}$ active elements, the equilibrium and compatibility conditions of an adaptive slab can be written as (cf. [34]):

$$Kd = f = f_{pas} + f_{act} \tag{3}$$

Here and in the following, the superscript # indicates the total number of the respective counting variable. The only exception is the designation *DOF*, as in this work no counting variable is used for it. $K \in \mathbb{R}^{DOF \times DOF}$ is the stiffness matrix, $d \in \mathbb{R}^{DOF}$ is the deformation vector, and $f \in \mathbb{R}^{DOF}$ is the force vector which is separated into forces for the passive state f_{pas} and forces of the active state f_{act}. Assuming small strains and displacements, a distinction can be made between three system states [11,43]: the "passive" state, which is the response of the structure to conventional loads (including self-weight and dead load), the "active" system state, which is the response of the structure caused by the actuation forces, and the "adaptive" state, which is taken as the superposition of passive and active states.

Using integrated fluidic actuators, forces are applied through a pair of faces located eccentrically to the cross-section neutral plane. A certain thickness of concrete is assumed to be covering the actuator, in order to achieve a homogeneous stress distribution and corrosion protection for the actuator. Figure 3 shows a single floor slab element of planar dimensions $l_{a,x}$, $l_{a,y}$. Indicated in red is the (pressurised) load application area A_a with a height of h_a. It is assumed that an actuation pushes the opposing faces pairwise apart, resulting in a pair of moments, similarly to what is shown in [22]. At this stage, the actuator concept is not fully defined since some of the parameters are an output of the process. Therefore, only moment pairs and no pressurised faces will be considered in the following.
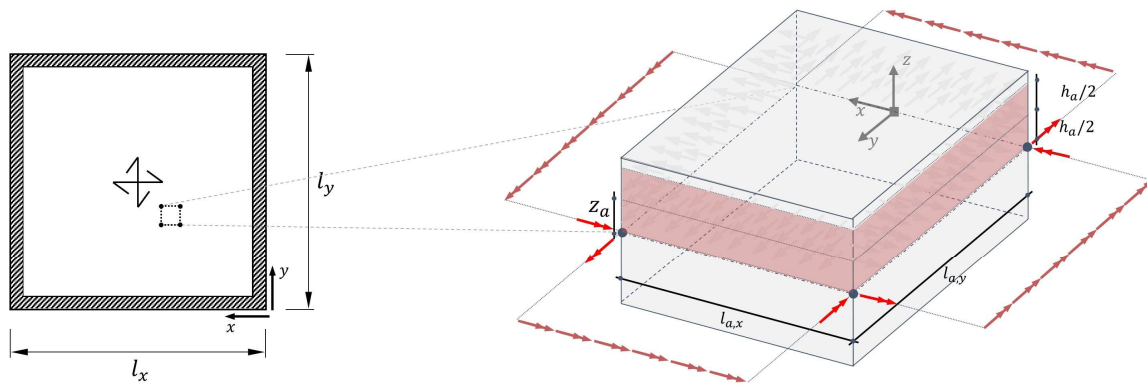
Figure 3. Unit cell of a slab section, with pressurised faces (red area) and resulting moments in x and y direction.

As long as the force pairs applied on the red faces (Figure 3) are only short-circuited along the actuator itself, the distance between the pair of moments can be varied in order to counteract the bending moment caused by the external load as needed. In this case, short-circuiting means that the resulting reaction forces cancel each other out through a connecting structure without leading to forces affecting the surrounding region of concrete. Three actuation modes are considered as shown in Figure 4, whereby the biaxial mode is a superposition of the two uniaxial modes. The labels 45° and 135° refer to the axis of the resulting moments with reference to the coordinate system shown in Figure 4. The force vector for the active state depends on the actuation mode employed (Figure 4).

(a)   (b)   (c)
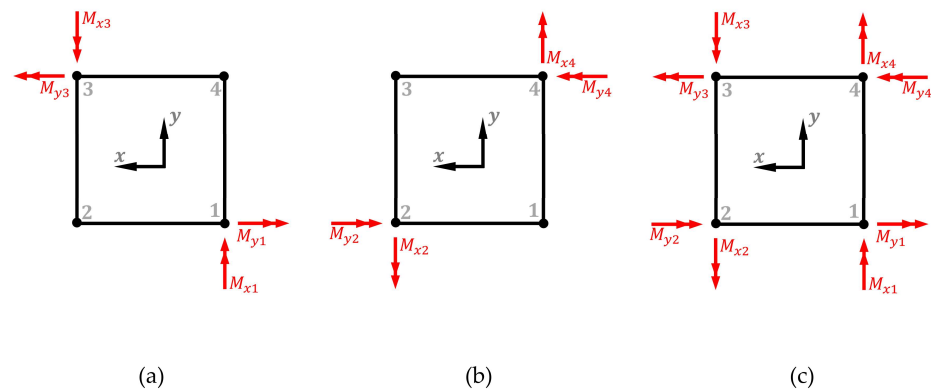
Figure 4. Actuation modes on single Elements—(**a**): uniaxial actuation 135°, (**b**): uniaxial actuation 45°, (**c**): biaxial Actuation.

The force vector in the active state can be written as follows (cf. [20]):

$$f_{act} = Au \tag{4}$$

The vector u contains the actuation input (see also Section 2.3). The matrix $A \in \mathbb{R}^{\text{DOF} \times i^\#}$ is denoted as the actuator allocation matrix. It collates the forces produced by the unit actuation of each individual element through a particular actuation mode column-wise:

$$A = \begin{bmatrix} a_1 & a_2 & \cdots & a_i & \cdots & a_{i^\#-1} & a_{i^\#} \end{bmatrix}, \tag{5}$$

For example, the column vector $a_{135°|1}$ corresponds to the uniaxial actuation mode 135° for element 1:

$$a_{135°|1} = [0 \overset{M_{x1}}{-\cos 45} \overset{M_{y1}}{-\sin 45} \cdots 0 \overset{M_{x4}}{\cos 45} \overset{M_{y4}}{\sin 45} \cdots 0 \overset{M_{xDOF}}{0} \overset{M_{yDOF}}{0}]^T \tag{6}$$

The force vector for the passive state can be generated in the same way, except that the entries of the A matrix must correspond to those of an out-of-plane load. In keeping with the concept of influence surfaces [33], only the active state is considered and f_{pas} is set to zero. Furthermore, only a unit actuation input is applied for all active elements. At this stage, the actuation input vector u can be formulated as the identity matrix of dimensions $\mathbb{R}^{i^{\#} \times i^{\#}}$, which can therefore be omitted [34]. Replacing Equation (3) in (4) yields the equation to compute the actuation influence matrix for displacements:

$$E_d = K^{-1}A \tag{7}$$

$$E_d = \begin{bmatrix} e_{d|1} & e_{d|2} & \cdots & e_{d|i} & \cdots & e_{d|i^{\#}-1} & e_{d|i^{\#}} \end{bmatrix} \tag{8}$$

The column vectors $e_{d|i} \in \mathbb{R}^{\text{DOF}}$ quantify the influence on nodal displacements (global coordinates) caused by unit actuation of the associated active element with the actuation mode that is being considered. To observe only the translational displacements w, the influence matrix of displacements $E_d \in \mathbb{R}^{\text{DOF} \times i^{\#}}$ can be reduced to $E_{d(w)} \in \mathbb{R}^{n^{\#} \times i^{\#}}$ by simply selecting every third global degree of freedom (cf. Equation (1)), $n^{\#}$ denotes the total number of element corner nodes. Each column vector $e_{d(w)|i} \in \mathbb{R}^{n^{\#}}$ quantifies the influence of a single active element on the nodal translational displacements w of the whole structure.

To obtain the actuation influence matrices for stress resultants, the strain–displacement matrices $B_b \in \mathbb{R}^{3 \times 12}$ and $B_s \in \mathbb{R}^{3 \times 12}$ as well as the stress–strain material matrices $C_b \in \mathbb{R}^{3 \times 3}$ and $C_s \in \mathbb{R}^{2 \times 2}$ are required for bending and shear respectively [40,42]. The formulation given in Equations (9)–(12) is for a single element following [40]. The coordinates must be transformed to the isoparametric coordinates of the gauss element according to [40,42].

$$B_b = \begin{bmatrix} 0 & \frac{\partial N_1}{\partial x} & 0 & 0 & \frac{\partial N_2}{\partial x} & 0 & 0 & \frac{\partial N_3}{\partial x} & 0 & 0 & \frac{\partial N_4}{\partial x} & 0 \\ 0 & 0 & \frac{\partial N_1}{\partial y} & 0 & 0 & \frac{\partial N_2}{\partial y} & 0 & 0 & \frac{\partial N_3}{\partial y} & 0 & 0 & \frac{\partial N_4}{\partial y} \\ 0 & \frac{\partial N_1}{\partial y} & \frac{\partial N_1}{\partial x} & 0 & \frac{\partial N_2}{\partial y} & \frac{\partial N_2}{\partial x} & 0 & \frac{\partial N_3}{\partial y} & \frac{\partial N_3}{\partial x} & 0 & \frac{\partial N_4}{\partial y} & \frac{\partial N_4}{\partial x} \end{bmatrix} \tag{9}$$

$$C_b = \frac{E \cdot t^3}{12 \cdot (1 + \mu^2)} \begin{bmatrix} 1 & \mu & 0 \\ \mu & 1 & \mu \\ 0 & 0 & \frac{1-\mu}{2} \end{bmatrix} \tag{10}$$

$$B_s = \begin{bmatrix} \frac{\partial N_1}{\partial x} & N_1 & 0 & \frac{\partial N_2}{\partial x} & N_2 & 0 & \frac{\partial N_3}{\partial x} & N_3 & 0 & \frac{\partial N_4}{\partial x} & N_4 & 0 \\ \frac{\partial N_1}{\partial y} & 0 & N_1 & \frac{\partial N_2}{\partial y} & 0 & N_2 & \frac{\partial N_3}{\partial y} & 0 & N_3 & \frac{\partial N_4}{\partial y} & 0 & N_4 \end{bmatrix} \tag{11}$$

$$C_s = \frac{5 \cdot E \cdot t}{12 \cdot (1 + \mu)} \begin{bmatrix} 1 & 0 \\ 0 & 1 \end{bmatrix} \tag{12}$$

A gauss node stress resultants vector can be calculated for the moments according to Equation (13) and for the shear forces according to Equation (14).

$$m^{(e')} = C_b^{(e')} B_b^{(e')} e_{d|i}^{(e)} \tag{13}$$

$$v^{(e')} = C_s^{(e')} B_s^{(e')} e_{d|i}^{(e)} \tag{14}$$

By iterating through the 4 gauss nodes while using the isoparametric coordinates (current gauss node coordinates) $\xi\prime$ and η' in the strain–displacement matrices of Equations (13) and (14), the stress resultant components ($m_{x'}$; $m_{y'}$; $m_{xy'}$; $v_{x'}$; $v_{y'}$) for the gaussian elements are obtained in turn. An example for $m_x^{(e')}$ and $v_x^{(e')}$ is given in Equations (15) and (16) [40,42].

$$m_x^{(e')} = \begin{bmatrix} m_{x|1'} & m_{x|2'} & m_{x|3'} & m_{x|4'} \end{bmatrix} \tag{15}$$

$$\boldsymbol{\nu}_x^{(e')} = \begin{bmatrix} \nu_{x|1'} & \nu_{x|2'} & \nu_{x|3'} & \nu_{x|4'} \end{bmatrix} \tag{16}$$

After calculating the stress resultants for each gauss element in turn, the values at the element corner nodes are obtained using bilinear extrapolation [42]. To avoid discontinuities between adjacent elements, the nodal stresses are averaged. For the averaging, the same weight is assigned to all elements that meet at a node [42]. Averaging reduces each stress resultant vector to one value per node, i.e., $\boldsymbol{m}_{x|i}, \boldsymbol{m}_{y|i}, \boldsymbol{m}_{xy|i}, \boldsymbol{v}_{x|i}, \boldsymbol{v}_{x|i} \in \mathbb{R}^{n^{\#}}$, where $n^{\#}$ denotes the total number of element corner nodes and i the respective active element.

To obtain actuation influence matrices for bending moments $\boldsymbol{E}_M \in \mathbb{R}^{n^{\#} \times i^{\#}}$ or shear forces $\boldsymbol{E}_V \in \mathbb{R}^{n^{\#} \times i^{\#}}$, the procedure in Equations (13)–(16) (including averaging) must be performed for each column vector $\boldsymbol{e}_{d|i}$ of the influence matrix $\boldsymbol{E}_d$. The stress resultant vectors generated are then collated column-wise into matrices as expressed in Equations (17) and (18).

$$\boldsymbol{E}_{M_x} = \begin{bmatrix} \boldsymbol{m}_{x|1} & \boldsymbol{m}_{x|2} & \cdots & \boldsymbol{m}_{x|i} & \cdots & \boldsymbol{m}_{x|i^{\#}-1} & \boldsymbol{m}_{x|i^{\#}} \end{bmatrix} \tag{17}$$

$$\boldsymbol{E}_{V_x} = \begin{bmatrix} \boldsymbol{v}_{x|1} & \boldsymbol{v}_{x|2} & \cdots & \boldsymbol{v}_{x|i} & \cdots & \boldsymbol{v}_{x|i^{\#}-1} & \boldsymbol{v}_{x|i^{\#}} \end{bmatrix} \tag{18}$$

To gain an understanding of the load-bearing behaviour of two-way slabs, it is useful to analyse the principal moments. With the calculated influence matrices $\boldsymbol{E}_{M_x}$, $\boldsymbol{E}_{M_y}$ and $\boldsymbol{E}_{M_{xy}}$, the influence matrices $\boldsymbol{E}_{m_1}$ and $\boldsymbol{E}_{m_2}$ for the two principal moment directions can be calculated. The influence matrices $\boldsymbol{E}_{m_1}$ and $\boldsymbol{E}_{m_2}$ for the two principal moments are obtained by successively collating the result of Equation (19) [44] applied to each column vector of $\boldsymbol{E}_{M_x}$, $\boldsymbol{E}_{M_y}$ and $\boldsymbol{E}_{M_{xy}}$ column-wise.

$$\boldsymbol{e}_{m_{1,2}} = \frac{\boldsymbol{m}_{x|i} - \boldsymbol{m}_{y|i}}{2\boldsymbol{m}_{xy|i}} \pm \frac{1}{\boldsymbol{m}_{xy|i}} \sqrt{\left(\frac{\boldsymbol{m}_{x|i} - \boldsymbol{m}_{y|i}}{2} \right)^2 + \boldsymbol{m}_{xy|i}^2} \tag{19}$$

2.2. Determining Suitable Actuation Modes

The optimal actuation mode depends on the control objective, e.g., reduction of deformations or homogenisation of bending moments. The selection of suitable actuation modes can be carried out on the basis of the computed influences. Summing the rows of the corresponding influence column vectors for each actuation mode k as indicated in Equations (20)–(21) yields a characteristic value of the influence of each element and actuation mode on the control objective *act* (e.g., $d(w), m_x$ etc.) under investigation. For example, if the control objective is displacement reduction, the rows of the individual column vectors of the influence matrix $\boldsymbol{E}_{d(w)}$ are summed.

$$e_{act|k,i} = \sum_{n=1}^{n^{\#}} e_{act|n,i k(actuation\ principle\ number)} \quad \begin{array}{l} n = 1, 2, \ \ldots, n^{\#} \ (counting\ variable\ for\ the\ element\ corner\ nodes\ ) \\ i = 1, 2, \ \ldots, i^{\#} \ (counting\ variable\ for\ the\ active\ elements\ ) \end{array} \tag{20}$$

$$\boldsymbol{e}_{act|k} = \begin{bmatrix} e_{act|k,1} & e_{act|k,2} & \cdots & e_{act|k,i} & \cdots & e_{act|k,i^{\#}-1} & e_{act|k,i^{\#}} \end{bmatrix} \tag{21}$$

For each actuation mode k, the row vectors $\boldsymbol{e}_{act|k,i} \in \mathbb{R}^{i^{\#}}$ are collated vertically into a matrix $\widetilde{\boldsymbol{E}}_{act} \in \mathbb{R}^{k^{\#} \times i^{\#}}$. Each row contains the summed influence of actuation mode k while

each column entry is the summed influence of an active element for the considered control objective at all element corner nodes, cf. Equation (22).

$$\widetilde{E}_{act} = \begin{bmatrix} e_{act|1} \\ e_{act|2} \\ \cdots \\ e_{act|k} \\ \cdots \\ e_{act|k^{\#}-1} \\ e_{act|k^{\#}} \end{bmatrix} \tag{22}$$

Using $\widetilde{E}_{act}$, the actuation mode with the highest influence can be determined for each active element. The maximum value per column indicates which actuation mode has the highest influence on the selected control objective at the respective active element (column index). In the following, the index of the actuation mode that has maximum influence at the respective active element i is denoted *kmax*.

The optimal actuation mode varies for the individual elements. Therefore, a new influence matrix $E_{d,comb}$ is assembled from the influence column vectors corresponding to the elements and actuation modes with the highest summed influence, using $\widetilde{E}_{act}$. For further processing (Section 2.3) and to visualise the selected actuation modes, it is also necessary to generate a new actuator allocation matrix of the combined actuation modes. For this purpose, the columns (active elements) of E_d and A corresponding to the actuation mode *kmax* on the selected control objective, are collated into the combined matrices $E_{d,comb}$ and A_{comb} respectively, as expressed in Equations (23) and (24).

$$E_{d,comb} = \begin{bmatrix} e_{d,kmax|1} & e_{d,kmax|2} & \cdots & e_{d,kmax|i} & \cdots & e_{d,kmax|i^{\#}-1} & e_{d,kmax|i^{\#}} \end{bmatrix} \tag{23}$$

$$A_{comb} = \begin{bmatrix} a_{kmax|1} & a_{kmax|2} & \cdots & a_{kmax|i} & \cdots & a_{kmax|i^{\#}-1} & a_{kmax|i^{\#}} \end{bmatrix} \tag{24}$$

2.3. Actuation Load, Adaption Level and Adaptive State

As described in [34], influence matrices can also be used to calculate the actuation forces required for a chosen adaptive nominal state y_{ada}. According to [33], Maxwell's theorem of reciprocal displacements also applies to elastic slabs. For example, consider the deformations in the passive state at a generic point *P(x,y)* caused by the external load and the deformations generated by a unit load (pair of moments) applied at a point *A(x,y)*. The actuation moment pair required to completely reduce the effect of the external load can be obtained from the ratio between the deformations in the passive and active state at point P. The approach presented in [34] to determine the actuation forces for truss and frame structures can be extended to floor slabs:

$$y_{ada} = y_{pas} + y_{act} = K^{-1}f_{pas} + E_{d,comb}u \tag{25}$$

Often the deformations caused by the permanent load (self-weight + dead load) are compensated by other means (e.g., pre-cambering). In these cases, it is possible to isolate the effect of variable loads (e.g., live load) by excluding the permanent load from the external load in the passive state f_{pas}.

Since influence matrices are typically not square and are therefore not invertible, the Moore–Penrose pseudoinverse, denoted with $(\cdot)^{+}$, is employed to compute the required actuation input u^{*}. The pseudoinverse is a generalisation of the inverse matrix to singular and non-square matrices [45]. Solving Equation (25) for u^{*} gives:

$$u^{*} = (E_{d,comb})^{+}\left(y_{ada} - y_{pas}\right) \tag{26}$$

The adaptive system state y_{ada}^* achievable with the actuation input u^* is then obtained by substituting u^* into Equation (25), as expressed in Equation (27). The same applies to the vector of actuation forces. Since the actuation modes considered in this work do not provide out-of-plane forces, there is no corresponding entry in A_{comb} for the translational degree of freedom, and therefore only actuation moments are included in the vector of actuation forces f_{act}^*.

$$y_{ada}^* = K^{-1}f_{pas} + E_{d,comb}u^* \tag{27}$$

$$f_{act}^* = A_{comb}u^* \tag{28}$$

2.4. Actuator Placement

When all structural elements are actuated, the adaptive state can typically be reached with high accuracy. However, this requires a high number of actuators. To reduce the complexity of the actuation system, it is sensible to reduce the number of actuators as much as possible. The reduction of actuators (i.e., the actuator placement) can be done based on the influence of the active element towards the attainment of the target adaptive state (Equation (20)). An iterative process is carried out by removing each element in turn and evaluating the effect on the target adaptive state.

The elements with the lowest influences are removed first. The minimum number of active elements is selected based on the desired control objective. For example, if vertical displacements are to be compensated, an upper (x_u) and lower (x_l) limit for the translational displacement w of each node is defined. The removal continues for elements with increasing influence until all elements are removed. It is not aborted after the upper or lower limit is reached in order to leave open the possibility (in a further step, which is not dealt with in this work) of analysing and discussing the procedure (cf. Equation (29), Section 4).

Due to the local effect that characterises the actuation with integrated fluidic actuators [22], it is useful to specify a removal direction. For example, if the external load is distributed on the floor slab, low-influence elements should be removed from the outside inwards to the diagonals and towards the centre of the slab. In cases where the external load is only distributed over one of the quadrants, the elements of the loaded quadrant should be removed last.

Elements are removed by filling zero entries into the corresponding column in $E_{d,comb}$. Each time an element is removed, the adaptive state $y_{ada,r}^*$ (Equation (27)) is computed with the updated $E_{d,comb}$ and collated into an output matrix $Y_{ada}^* \in \mathbb{R}^{\text{DOF} \times \text{r}^\#}$ where $r^\#$ denotes the total number of removed elements.

$$Y_{ada}^* = \begin{bmatrix} y_{ada,1}^* & y_{ada,2}^* & \cdots & y_{ada,r}^* & \cdots & y_{ada,r^\#-1}^* & y_{ada,r^\#}^* \end{bmatrix} \tag{29}$$

Due to the order of the degrees of freedom (Equation (1)), the matrix for the adaptive state for translational displacements $Y_{ada(w)}^* \in \mathbb{R}^{n^\# \times i^\#}$ can be determined by filtering every third column entry of Y_{ada}^*. The minimum number of active elements is equal to the total number of active elements minus the lowest column index from $Y_{ada(w)}^*$ in which the target displacement bounds are exceeded. The reduced influence matrix $E_{d,comb,r}$, which corresponds to the configuration with the minimum number of actuators, is used to compute the adaptive state and the required actuation moments using Equations (26)–(28).

2.5. Defining Pressure Levels

As described in Section 2.1, actuation moments are produced by applying pressure to pairs of faces, resulting in an actuation moment (cf. [22], Figure 3). Given f_{act}^* from Equation (28), the calculation of the pressure p_{act}^* is based on Equation (30) which was

formulated and experimentally validated in [22] for beams. $A_{a,x}$ is the load application area in the x direction and z_a is the inner lever arm (Figure 3).

$$p^*_{act} = \frac{f^*_{act}}{A_{a,x} \cdot z_a}$$ (30)

The moment curve between a pair of actuation moments is assumed to be constant. As discussed in Section 2.1, this constant moment curve can be induced across multiple elements.

Adjacent elements that are actuated through approximately the same pressure are thought of as forming a pressure level. Consider the example of biaxial actuation shown in Figure 5. Since the actuation moments at adjacent nodes cancel each other out (Figure 5a), the combined elements are equivalent to a larger active element (cf. Figure 5b). This shifts the pairs of faces to the outer edges of the larger active element. This means that the number of active elements does not have to be the same as the actual number of actuators. The active elements are employed to define the active region in which the actuators will be placed. Furthermore, grouping active elements through pressure levels is useful for limiting the necessary number of valves of the hydraulic unit. The number of pressure levels can be chosen, for example, on the basis of the available hydraulic unit. The pressure levels correspond to an even distribution of the pressures over the maximum pressure range. The pressure range corresponds to the maximum required pressure or a selected pressure limit. A pressure limit can be chosen, for example, on the basis of requirements from the actuator concept as well as on the basis of material properties such as the concrete compressive strength. When reducing the number of active elements to obtain the actuator placement region, the remaining active elements are required to apply higher pressure to compensate for the missing elements. In some cases, this can lead to an extraordinary increase in the highest pressure levels. If a significantly high step occurs between individual pressures after sorting them, all pressures beyond the selected step are limited to the nearest smaller pressure level.

(a)   (b)
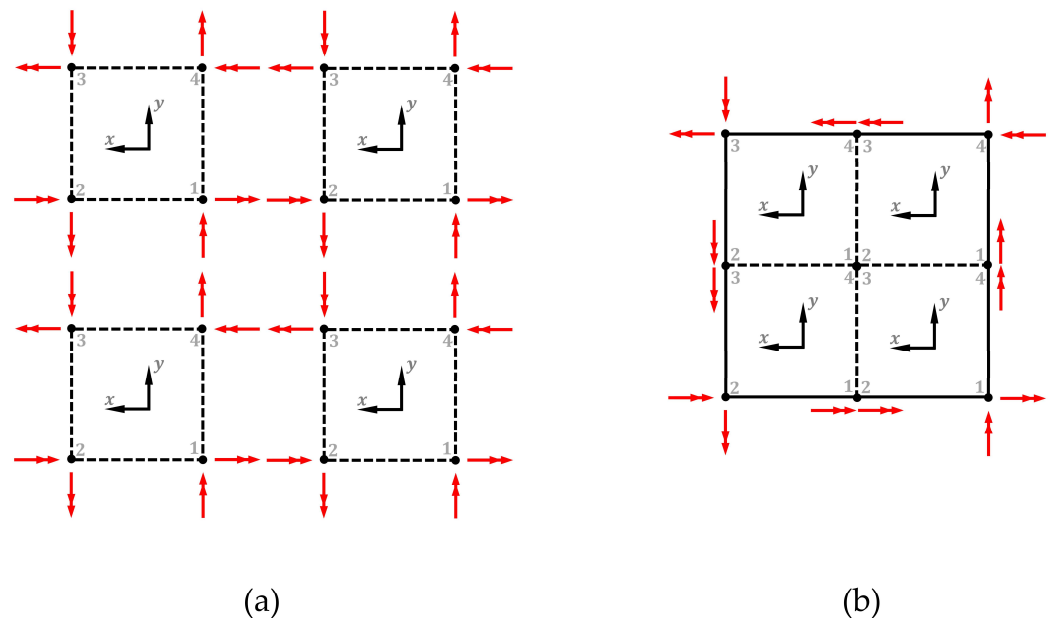
Figure 5. (**a**) Superposition of actuation moments between adjacent elements using biaxial actuation. (**b**) Result of the superposition—larger active element.

3. Results

In the following, the application of the method formulated in Section 2 is applied to a case study of a simply supported slab. A summary of this procedure can be found in

Appendix A. Dimensions and material properties, indicated in Table 1, have been selected on the basis of planned experimental testing and available resources. The control objective is the reduction of displacements. The nodal translational displacements are constrained along all edges. The floor slab is discretised in 400 elements as shown in Figure 6. The element size was chosen based on the mesh convergence study shown in Figure 7. A comparison of the numerically determined translational displacements and moments in *x*- and *y*-direction at slab midspan with the analytically calculated values according to Czerny [46] yields a deviation of around 10%. Due to the relatively small values (cf. Section 3.4), this is considered to be sufficiently accurate for the presentation of the method. The simulations have been performed in Python 3.7.8.

Table 1. Slab dimensions and material properties.

Properties	Value	Unit
Span $l_x = l_y$	2	m
Thickness	0.1	m
Elementsize $l_{a,x} = l_{a,y}$	0.1	m
E-modulus	30	GPa
Poisson's ratio	0.2	-
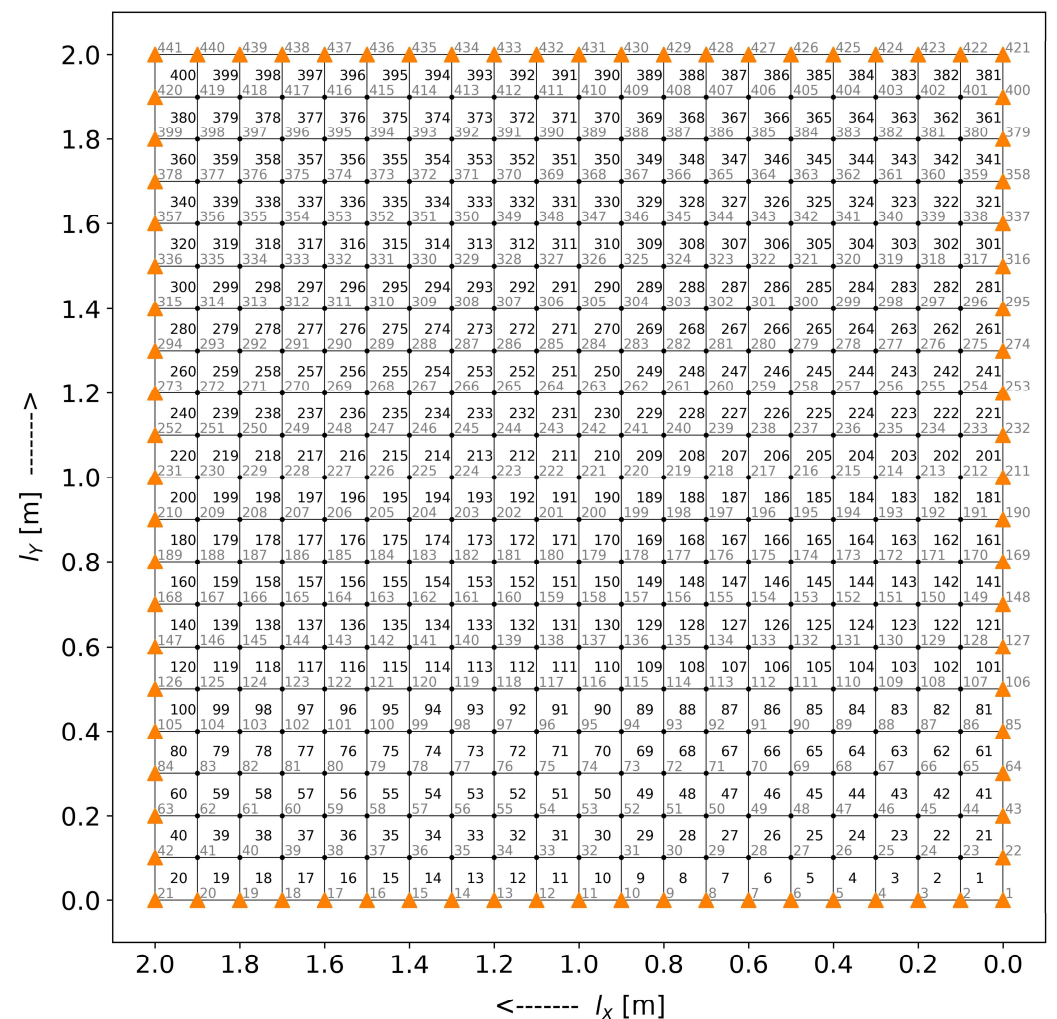
Figure 6. Finite element mesh with element (black) and node (grey) number as well as boundary conditions.
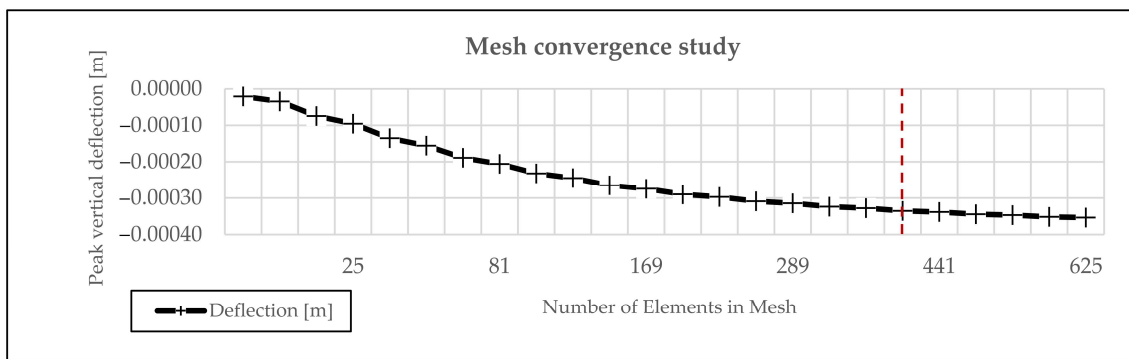
Figure 7. Mesh convergence study, red dashed line indicates the number of elements for the chosen element size of 0.1 m × 0.1 m.

3.1. Influence Matrices

It is useful to compare the individual plots of the columns of the influence matrices for each actuation mode in the case of the chosen control objective, the columns of the influence matrix $E_{d(w)}$. To compute the resulting displacement response in the passive state, a similar influence matrix can be built by applying a unitary out-of-plane load at every element corner node of a single element. Figure 8 shows an example of three plotted columns for the passive (a–c) and active state (d–f). In this example three application points are chosen: the centre of the slab, the centre of a diagonal and the principal axes related to one quadrant.

In the passive system state, the highest influences are indicated in dark blue (negative deflection) and, in the active state, they are indicated in bright yellow (positive deflection). The response is more pronounced in the immediate vicinity of the load application points or position of the active elements (marked with pink dots and arrows) and then decreases rapidly. The influence extends over a smaller region when load application points (or the position of the active element) are considered closer to the edges.
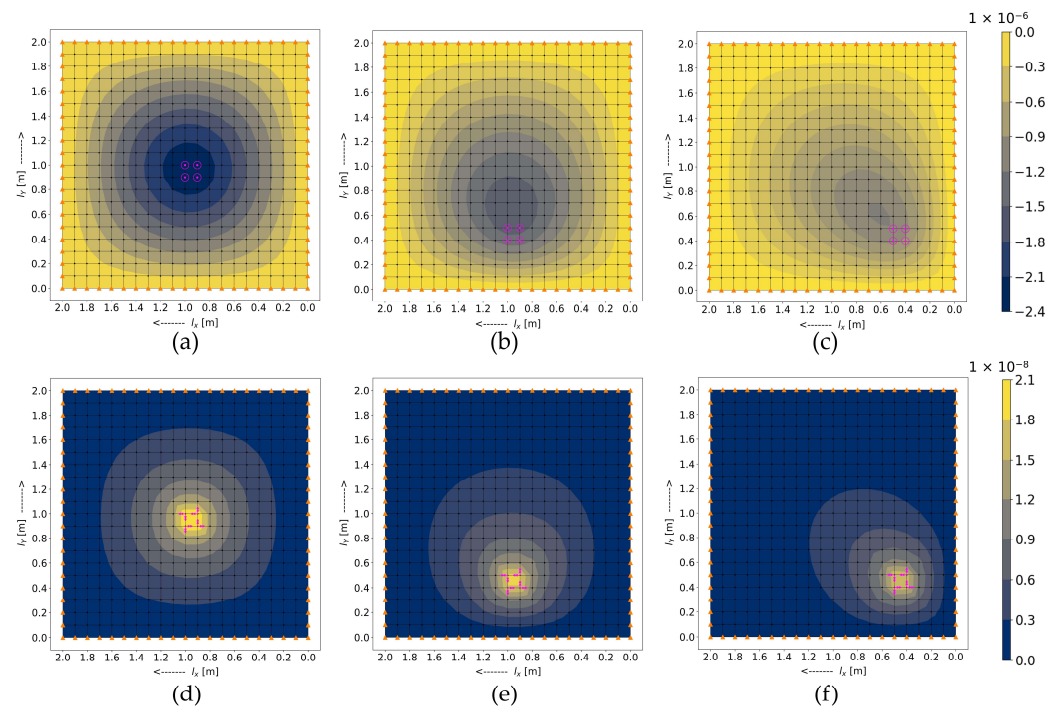
Figure 8. From left to right displacements w in m, near the centre of the slab, near the centre of the principal axes and the diagonal related to one quadrant, for a quasi-unitary load (**a–c**) as well as a biaxial actuation (**d–f**). Loading marked in pink.

3.2. Combining Actuation Modes

Figure 9 shows the plot of the summed influences on translational displacements w under biaxial actuation (a), 45° (b) and 135° (c) uniaxial actuation (cf. Section 2.2) for all elements. In red areas, the influence on the control objective is the largest, in green areas it is negligible and in purple areas it is negative, i.e., actuation causes downward displacements.
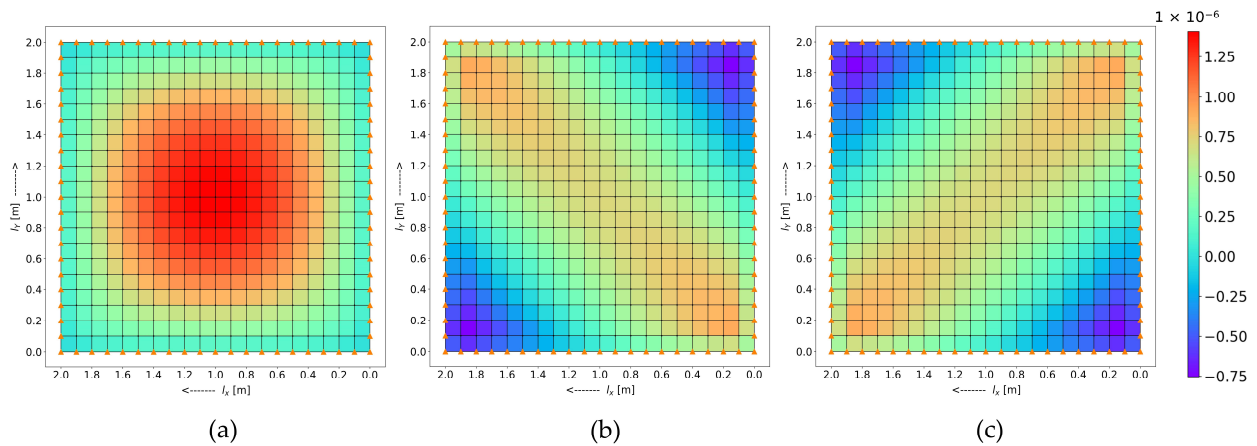
Figure 9. Summed influences over all elements on the displacements w of a biaxial actuation (**a**), 45° (**b**) as well as 135° (**c**) uniaxial actuation.

Figure 9 shows that the biaxial actuation mode is most efficient in the centre of the slab but has almost no effect in the corners. The uniaxial actuation modes affect the deformations along the diagonals and mostly towards the corners, according to their alignment with the principal moment m_1. It is important to align uniaxial actuation correctly with respect to the principal moment m_1. The principal moments change sign at the corners, so actuation has a negative effect on the displacements w. Figure 10 shows the actuation modes selected after applying Equations (20)–(24).
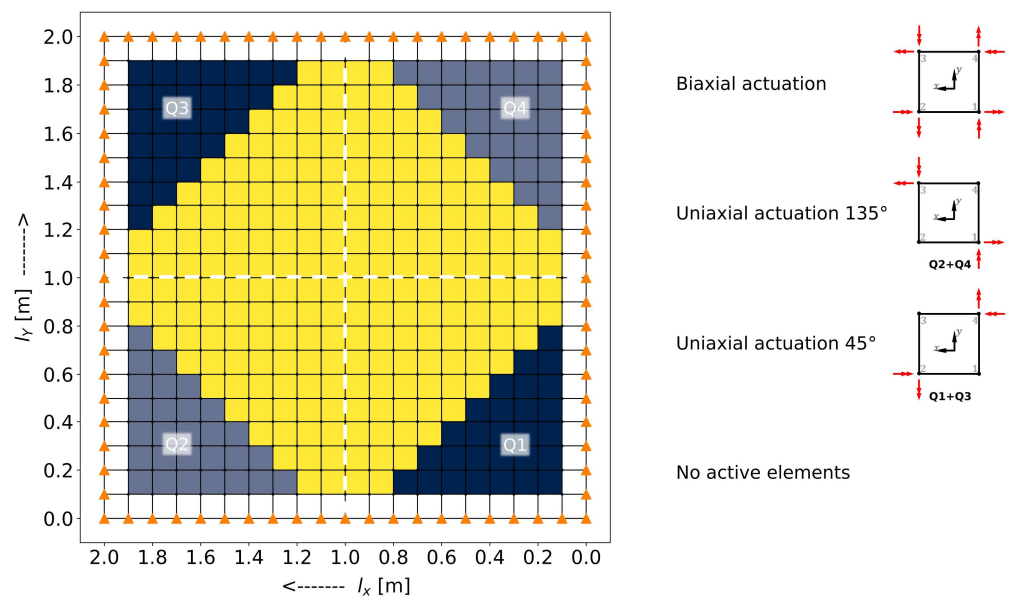
Figure 10. Distribution of actuation principles.

3.3. Actuation Load and Adaptation Level

To obtain measurable displacements under the considered dimensions and material properties (Table 1), a distributed load of 15 kN/m² is applied. The active moments required to compensate displacements w as well as rotations φ_x and φ_y are computed

with Equations (25)–(27) for a distribution of actuation modes according to Figure 10. The required actuation pressures are indicated in Figure 11. If all the coloured elements in Figure 10 are active, the maximum required pressure is approximately 76 bar. The required pressure is the highest in the proximity of the sign change of the principal moment m_1. The pressure is computed with Equation (30). The chosen values $A_{a,x} = 0.003 \text{ m}^2$ (0.1 m × 0.03 m) and $z_a = 0.015$ m correspond to the maximum size per element to obtain a concrete cover of 2 cm.
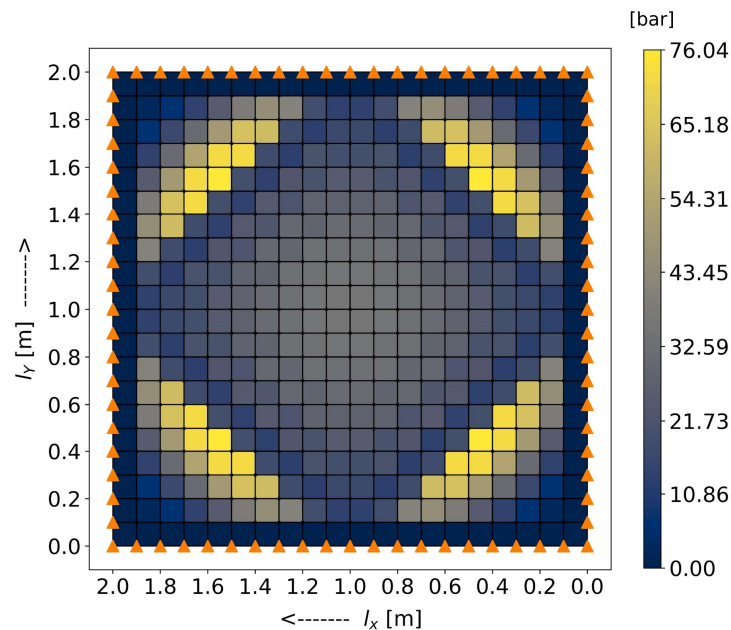
Figure 11. Actuation pressures to compensate for the displacements caused by a distributed load of 15 kN/m².

3.4. Number of Necessary Active Elements

If a permissible range is defined for the displacements w, not all active elements are required. For the case study under consideration, the application of the procedure described in Section 2.4 leads to a required number of active elements of 232 (out of a total of 400). Figure 12 shows a zoomed-out view of the matrix $Y^*_{ada(w)} \in \mathbb{R}^{n^\# \times i^\#}$. The individual entries that lie within the permissible deformation range of $x_u = 1 \times 10^{-5}$ to $x_l = -1 \times 10^{-5}$ are highlighted in red. The representation is structured in such a way that one element is removed per column from left to right. From top to bottom, the node number is listed in ascending order. The set permissible range can no longer be complied with when an active element is removed from the area where the principal moment m_1 is close to zero.

The maximum value of the displacement in the passive state w_{pas} is 3.4×10^{-4} m. When all elements are active, the maximum displacement in the adaptive state w_{ada} is 0.032×10^{-4} m (a reduction of 99.9%). After removing 168 active elements (Figure 13) the maximum displacement in the adaptive state is only 0.074×10^{-4} m (a reduction of 97.8%), due to the strict chosen displacement bounds.

	active elements 232	active elements 231
w at node no. 85	0	0
w at node no. 86	-4.03050×10^{-6}	-5.43813×10^{-6}
w at node no. 87	-6.51440×10^{-6}	-9.29257×10^{-6}
w at node no. 88	-6.99307×10^{-6}	-1.01272×10^{-5}
w at node no. 89	-5.69843×10^{-6}	-7.70332×10^{-6}
w at node no. 90	-3.48294×10^{-6}	-4.12437×10^{-6}
w at node no. 91	-8.51841×10^{-7}	-7.15088×10^{-7}
w at node no. 92	-8.45662×10^{-7}	-7.65491×10^{-7}
w at node no. 93	-1.10048×10^{-6}	-1.04941×10^{-6}
w at node no. 94	-1.28396×10^{-6}	-1.26272×10^{-6}
w at node no. 95	-1.36153×10^{-6}	-1.34924×10^{-6}
w at node no. 96	-1.28396×10^{-6}	-1.27878×10^{-6}
w at node no. 97	-1.10048×10^{-6}	-1.09551×10^{-6}
w at node no. 98	-8.45662×10^{-7}	-8.42878×10^{-7}
w at node no. 99	-8.51841×10^{-7}	-8.44335×10^{-7}
w at node no. 100	-3.48294×10^{-6}	-3.47752×10^{-6}
w at node no. 101	-5.69843×10^{-6}	-5.68894×10^{-6}
w at node no. 102	-6.99307×10^{-6}	-6.99034×10^{-6}
w at node no. 103	-6.51440×10^{-6}	-6.51608×10^{-6}
w at node no. 104	-4.03050×10^{-6}	-4.03328×10^{-6}
w at node no. 105	0	0
w at node no. 106	0	0
w at node no. 107	-4.62642×10^{-6}	-5.59241×10^{-6}
w at node no. 108	-6.95291×10^{-6}	-9.29859×10^{-6}
w at node no. 109	-6.11119×10^{-6}	-1.04173×10^{-5}
w at node no. 110	-3.48294×10^{-6}	-5.68597×10^{-6}

Figure 12. Zoomed-out display of the matrix $Y^*_{ada(w)}$. The displacements w at the element corner nodes that lie outside the permissible range are highlighted in red.
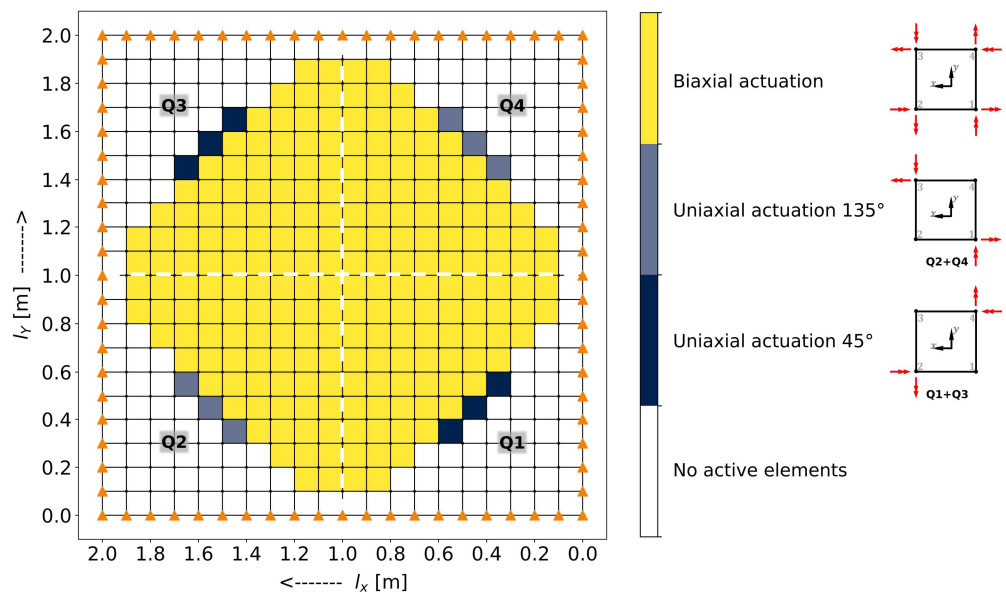
Figure 13. Distribution of actuation principles after removing 168 active elements.

3.5. Defining Pressure Levels

A reduction in the number of active elements can result in a large increase in the required actuation pressure. Figure 14a shows the required actuation pressures to satisfy the displacement bounds set in Section 3.4. Compared to the case in which all elements are active (Figure 11), the maximum pressure increases from 76 bar to 164 bar. To further reduce the number of actuators, elements with a similar pressure are combined through pressure levels (Section 2.5). In addition, since the pressure only increases significantly for some of the elements, a pressure limit is introduced. Six pressure levels are defined, since the hydraulic unit that will be used for testing has six valves. For the general pressure levels, this results in steps of roughly 10 bar. The pressure level of the few active elements with extreme values is manually limited to the highest pressure level. The actuation pressure

plot for this case is shown in Figure 14b. The maximum displacement for this variation is 0.42×10^{-4} m ($w_{pas} = 3.4 \times 10^{-4}$ m, reduction of 87.6%).

(a)

(b)
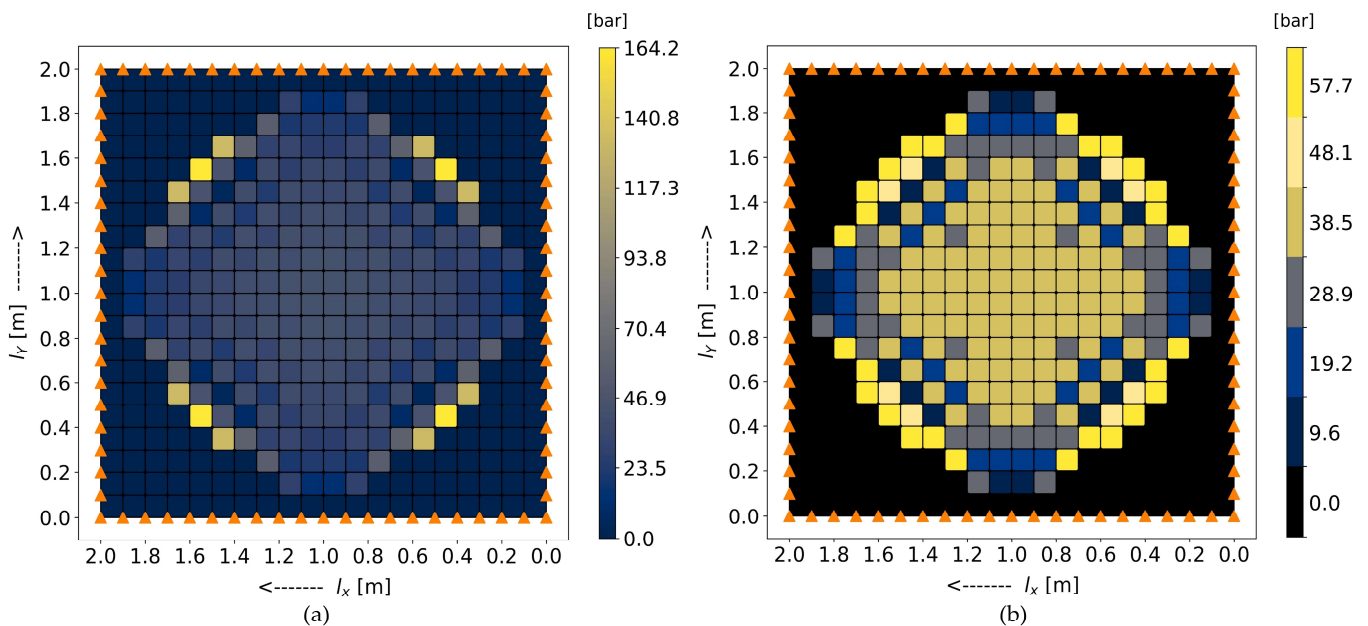
Figure 14. (**a**) Actuation pressures after reduction of the active elements. (**b**) Actuation pressures using six pressure levels, including pressure limit.

4. Discussion

The concept of integrated fluidic actuation has already been validated on a large-scale beam in [18]. In this study, the underlying approach of counteracting moments caused by external loads with opposing active moments has been extended to floor slabs. The directionality of the load transfer in two-way slabs increases the complexity. Influence matrices are employed to determine the location of the active elements and the required actuation forces to satisfy a chosen control objective.

The simplification of the 2-dimensional plate theory does not allow an evaluation of the stress in thickness direction since the stress curve from pressurised eccentric faces does not correspond to the linear stress curve of the plate theory. However, the knowledge gained regarding the orientation and intensity of the actuation moments, as well as the possibility of identifying actuator design spaces (pattern from pressure levels) with reduced computation time, justifies this approach. Stresses in the thickness direction can be evaluated separately, since individual variations still have to be checked during the development of the actuator concept.

In general, practical implementation will have to be tested to appreciate the feasibility of the method proposed in this paper. This includes the necessary proof that the distance between the pairs of moments can be increased by an appropriate actuator structure. The exact implementation (1 actuator = 1 active element or 1 pressure level field) would mean that there is no concrete between the individual pressurised faces. In addition, the actuator requires a construction space (enclosure, connecting elements, etc.) where no force can be applied on the concrete. This issue can be solved by allowing gaps between the active elements (or pressure fields). The applied pressure is distributed in plane, resulting in actuation moments that are not just directly at the pressurised faces. The distances between individual actuators can be selected based on the decay lengths of the applied in-plane stresses (cf. [22]). These adjustments lead to a smaller load application area A_a. In practical implementation, the maximum pressure required for displacement compensation will therefore be higher, with expected values of about 100 bar. In the case study presented in this work, the use of pressure barriers has a larger impact on the deviation from the desired displacement bounds than the reduction of active elements. This means that if a bigger

area (with more combined active elements) is actuated, smaller inaccuracies can also be compensated for.

The effect of the actuation modes on actuator placement and determination of the minimum number of active elements for different control objectives will be the subject of future work. A review of $Y^*_{ada(w)}$ shows that there are still some active elements that can be removed without affecting compliance with the deformation criteria. Further work will also analyse and improve the removal process.

Although slabs are typically dimensioned based on deformation limits and very good results for deformation reduction at relatively low pressures have been demonstrated in this study, it remains to be proven that the basic goal behind the adaptive slab, i.e., savings in mass and resources, can be achieved. Especially since no statement can be made about the mass of the actuators at this point in the design phase.

5. Conclusions

This study presents an extension of the use of influence matrices from trusses and beams to two-way slabs with integrated fluidic actuators. The actuation influence matrices are employed to place the actuators as well as to determine preliminary requirements for the actuator concept. It has been shown that the characteristic value of the summed influences is a useful indicator to choose suitable actuation modes. Through the determination of pressure levels, optimal position and forces of the actuators can be obtained for a chosen control objective including the distance between the pair of faces (design space) of the fluidic actuators. Through the load case independent analysis, it was shown that biaxial actuation in the centre of the slab and uniaxial actuation along the diagonals is advantageous. Furthermore, the paper illustrates that actuation in the corner areas is not necessary for displacement compensation of a uniformly distributed load. This highlights that adaptive slabs require specifically designed actuators instead of industry standard ones to reduce the number of actuators and to achieve a good performance. Moreover, it was presented that with a gradation of just six pressure levels, displacements from a uniformly distributed load can be reduced by more than 85%. Future work will test the feasibility of the presented method in this paper and general practical applicability of adaptive slabs through experimental testing.

Glossary

Sub- and Superscripts:

#	indicates the total number of the respective counting variable
*	indicates that the vector or matrix refers to the required target state
DOF	degrees of freedom
(e)	single element, evaluation at the element corner nodes
(e')	single "gauss" element, evaluation at the gauss nodes
i	counting variable for the active elements $(i = 1, 2, \ldots, i^{\#})$

k	counting variable for the actuation modes
$kmax$	index of the actuation mode that has maximum influence at the respective active element
n	counting variable for the element corner nodes $\left(n = 1, 2, \ldots, n^{\#}\right)$
r	counting variable for the number of removed elements $\left(r = 1, 2, \ldots, r^{\#}\right)$

Vectors:

$\boldsymbol{a}_i \in \mathbb{R}^{\mathrm{DOF}}$	column vector of the actuator allocation matrix. Including the actuation mode, e.g., corresponds to the uniaxial actuation mode, e.g., $\boldsymbol{a}_{135°	1}$ for element 1
$\boldsymbol{d}^{(e)}. \in \mathbb{R}^{12}$	element deformation vector
$\boldsymbol{d} \in \mathbb{R}^{\mathrm{DOF}}$	global deformation vector
$\boldsymbol{e}_{act	k} \in \mathbb{R}^{i^{\#}}$	row vector of the summed rows of the corresponding influence column vectors of each element and actuation mode on the control objective
$\boldsymbol{e}_{d	i} \in \mathbb{R}^{\mathrm{DOF}}$	column vector of the actuation influence matrix for displacements
$\boldsymbol{e}_{d(w)	i} \in \mathbb{R}^{n^{\#}}$	column vector of the actuation influence matrix for translational displacements w
$\boldsymbol{e}_{m_{1,2}} \in \mathbb{R}^{n^{\#}}$	column vector of actuation influence matrices for the two principal moment directions
$\boldsymbol{f} \in \mathbb{R}^{\mathrm{DOF}}$	global force vector
$\boldsymbol{f}^{(e)} \in \mathbb{R}^{12}$	element force vector
$\boldsymbol{f}_{act}^* \in \mathbb{R}^{\mathrm{DOF}}$	force vector of the required actuation moments
$\boldsymbol{f}_{act}^* \in \mathbb{R}^{\mathrm{DOF}}$	global force vector for the active state
$\boldsymbol{f}_{pas} \in \mathbb{R}^{\mathrm{DOF}}$	global force vector for the passive state
$\boldsymbol{m}^{(e')} \in \mathbb{R}^4$	gauss node stress resultant vector for the bending moments
$\boldsymbol{p}_{act}^* \in \mathbb{R}^{\mathrm{DOF}}$	actuation pressure vector
$\boldsymbol{u}^* \in \mathbb{R}^{\mathrm{DOF}}$	required actuation input vector, for a target state
$\boldsymbol{u} \in \mathbb{R}^{\mathrm{DOF}}$	actuation input vector
$\boldsymbol{v}^{(e')} \in \mathbb{R}^4$	gauss node stress resultant vector for the shear forces
$\boldsymbol{y}_{act} \in \mathbb{R}^{\mathrm{DOF}}$	output vector for the active nominal state
$\boldsymbol{y}_{ada}^* \in \mathbb{R}^{\mathrm{DOF}}$	output vector for the adaptive system state achievable with the actuation input $\boldsymbol{u}^*$
$\in \mathbb{R}^{\mathrm{DOF}}$	output vector for the adaptive system state achievable with the actuation input $\boldsymbol{u}^*$ and the current number of active elements
$\boldsymbol{y}_{ada} \in \mathbb{R}^{\mathrm{DOF}}$	output vector for the adaptive nominal state
$\boldsymbol{y}_{pas} \in \mathbb{R}^{\mathrm{DOF}}$	output vector for the passive nominal state

Matrices:

$\boldsymbol{A} \in \mathbb{R}^{\mathrm{DOF} \times i^{\#}}$	actuator allocation matrix
$\boldsymbol{A}_{comb} \in \mathbb{R}^{\mathrm{DOF} \times i^{\#}}$	actuator allocation matrix of the combined actuation modes
$\boldsymbol{B}_b \in \mathbb{R}^{3 \times 12}$	strain–displacement matrices for bending
$\boldsymbol{B}_s \in \mathbb{R}^{3 \times 12}$	strain–displacement matrices for shear
$\boldsymbol{C}_b \in \mathbb{R}^{3 \times 3}$	stress–strain material matrices for bending
$\boldsymbol{C}_s \in \mathbb{R}^{2 \times 2}$	stress–strain material matrices for shear
$\widetilde{\boldsymbol{E}}_{act} \in \mathbb{R}^{k^{\#} \times i^{\#}}$	actuation influence matrix for the summed influences of each element and actuation mode on the control objective
$\boldsymbol{E}_d \in \mathbb{R}^{\mathrm{DOF} \times i^{\#}}$	actuation influence matrix for displacements
$\boldsymbol{E}_{d,comb} \in \mathbb{R}^{\mathrm{DOF} \times i^{\#}}$	actuation influence matrix for displacements of the combined actuation modes with the highest summed influence
$\boldsymbol{E}_{d,comb,r} \in \mathbb{R}^{\mathrm{DOF} \times i^{\#}}$	actuation influence matrix for displacements of the combined actuation modes with the highest summed influence and the minimum number of active elements to stay within the target state bounds
$\boldsymbol{E}_{d(w)} \in \mathbb{R}^{n^{\#} \times i^{\#}}$	actuation influence matrix for translational displacements w
$\boldsymbol{E}_M \in \mathbb{R}^{n^{\#} \times i^{\#}}$	actuation influence matrix for bending moments
$\boldsymbol{E}_{m_1}$ and $\boldsymbol{E}_{m_2} \in \mathbb{R}^{n^{\#} \times i^{\#}}$	actuation influence matrices for the two principal moment directions
$\boldsymbol{E}_V \in \mathbb{R}^{n^{\#} \times i^{\#}}$	actuation influence matrix for shear forces
$\boldsymbol{K} \in \mathbb{R}^{\mathrm{DOF} \times \mathrm{DOF}}$	global stiffness matrix

k	counting variable for the actuation modes
$Y^*_{ada} \in \mathbb{R}^{\mathrm{DOF} \times i^\#}$	output matrix for the adaptive system state achievable with the actuation input u^* and the current number of active elements
$Y^*_{ada(w)} \in \mathbb{R}^{n^\# \times i^\#}$	output matrix for the translational displacements in the adaptive system state achievable with the actuation input u^* and the current number of active elements

Symbols:

$(\cdot)^+$	Moore–Penrose pseudoinverse
φ_x and φ_y	rotational degrees of freedom
A_a	load application area
$e_{act|k,i}$	summed influence of a single element on the control objective for the respective actuation mode
$e_{act|n,i}$	influence of a single element on the control objective at the respective element corner node
h_a	height of the load application area
$l_{a,x}$ and $l_{a,y}$	edge length of a single slab element in x and y direction. Applies also when using pressure levels to form a single larger active element.
l_x and l_y	span width of the slab in x and y direction
w	translational displacement
x_u	upper limit for the translational displacement w of each node
x_l	lower limit for the translational displacement w of each node
z_a	inner lever

Appendix A

A summary of the procedure described in Section 2.1–2.5 is given in Figure A1 as a flow chart. First of all, the influence matrices for each actuation mode need to be calculated. Summing the rows of the influence column vectors yields a characteristic value to determine suitable actuation modes. After assigning a load case and setting an adaptive target state, the adaptive system state can be calculated. By removing active elements with the lowest influence in turn the minimum number of active elements can be determined. Assigning pressure levels and setting a pressure limit leads to possible distances for the actuation faces.
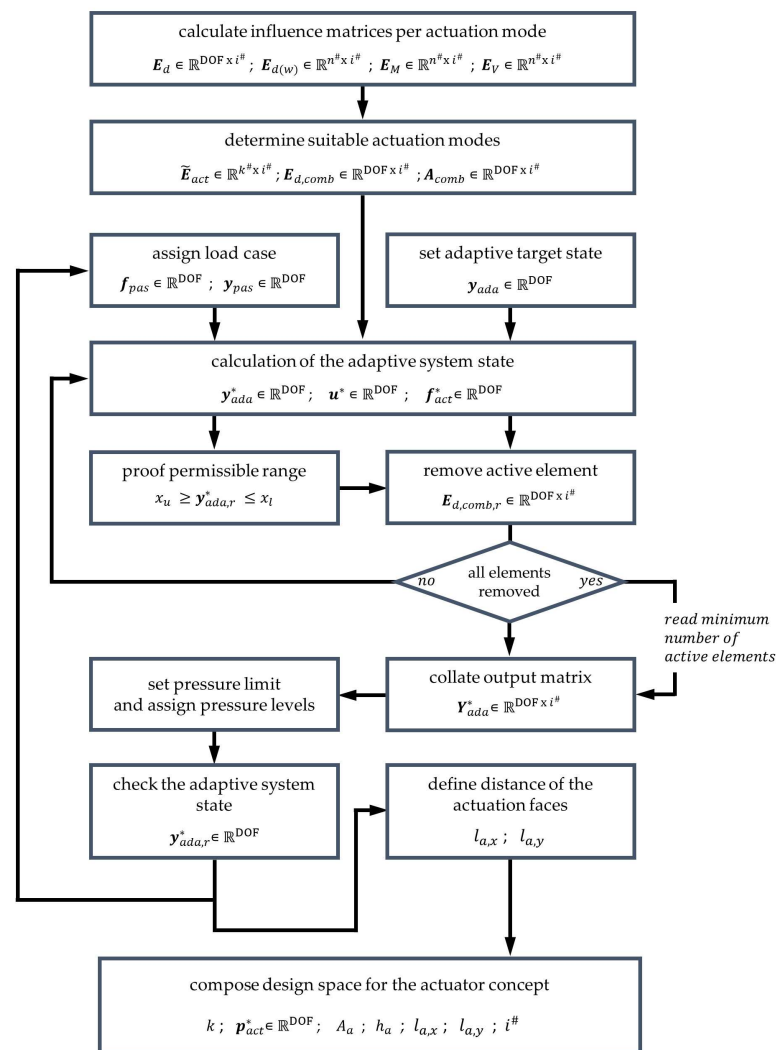
Figure A1. Summary of the procedure described in Section 2.1, Section 2.2, Section 2.3, Section 2.4, Section 2.5.

References

1. Sobek, W. *Non Nobis—Über das Bauen in der Zukunft, Bd. 1: Ausgehen Muss Man von Dem, Was Ist*; av edition: Stuttgart, Germany, 2022; ISBN 978-3-89986-369-7.
2. UNEP. *2020 Global Status Report for Buildings and Construction: Towards a Zero-Emission, Efficient and Resilient Buildings and Construction Sector*; UNEP: Nairobi, Kenya, 2020.
3. BKI. *BKI Kostenplaner 2021—Statistik Plus, Positionen*; Baukosteninformationszentrum Deutscher Architektenkammern GmbH: Stuttgart, Germany, 2021.
4. Berger, T.; Prasser, P.; Reinke, H.G. Einsparung von Grauer Energie bei Hochhäusern. *Beton- und Stahlbetonbau* **2013**, *108*, 395–403. [CrossRef]
5. Stepan, K. Vergleichende Untersuchungen von Deckensystemen des Stahlbeton-Skelettbaus. Ph.D. Dissertation, Technische Universität München, München, Germany, 2004.
6. Scrivener, K.L.; Kirkpatrick, R.J. Innovation in use and research on cementitious material. *Cem. Concr. Res.* **2008**, *38*, 128–136. [CrossRef]
7. Peduzzi, P. *Sand, Rarer Than One Thinks: UNEP Global Environmental Alert Service*; UNEP: Nairobi, Kenya, 2014.
8. WWF Deutschland. *Klimaschutz in der Beton- und Zementindustrie: Hintergrund und Handlungsoptionen*; WWF Deutschland: Berlin, Germany, 2019; pp. 7–11.
9. Zilch, K.; Rogge, A. Bemessung von Stahlbeton- und Spannbetonbauteilen im Brücken- und Hochbau. *Beton-Kalender* **2004**, *93*, 281–283.
10. Schmeer, D.; Sobek, W. Gradientenbeton. In *Beton-Kalender 2019: Parkbauten Geotechnik und Eurocode 7, 108. Jahrgang*; Bergmeister, K., Fingerloos, F., Wörner, J.-D., Eds.; Ernst et Sohn: Berlin, Germany, 2019; pp. 455–476. ISBN 9783433032428.
11. Sobek, W. Ultra-lightweight construction. *Int. J. Space Struct.* **2016**, *31*, 74–80. [CrossRef]

12. Ostertag, A.; Dazer, M.; Bertsche, B.; Schlegl, F.; Sawodny, O. Reliable Design of Adaptive Load-Bearing Structures with Focus on Sustainability. In Proceedings of the 30th European Safety and Reliability Conference (ESREL), Venice, Italy, 2–5 November 2020; pp. 4703–4710.

13. Ostertag, A. *Zuverlässigkeit, Sicherheit und Nachhaltigkeit Adaptiver Tragwerke*; Institut für Maschinenelemente: Stuttgart, Germany, 2021.

14. Yao, J.T.P. Concept of structural control. *J. Struct. Div. (ASCE)* **1972**, *98*, 1567–1574. [CrossRef]

15. Domke, H.; Backé, W.; Meyr, H.; Hirsch, G.; Goffin, H. Aktive Verformungskontrolle von Bauwerken. *Bauingenieur* **1981**, *56*, 405–412.

16. Soong, T.T.; Manolis, G.D. Active structures. *J. Struct. Eng.* **1987**, *113*, 2290–2302. [CrossRef]

17. Neuhäuser, S.; Weickgenannt, M.; Witte, C.; Haase, W.; Sawodny, O.; Sobek, W. Stuttgart Smartshell—A full scale prototype of an adaptive shell structure. *J. Int. Assoc. Shell Spat. Struct.* **2013**, *54*, 259–270.

18. Burghardt, T.; Kelleter, C.; Bosch, M.; Nitzlader, M.; Bachmann, M.; Binz, H.; Blandini, L.; Sobek, W. Investigations of a large-scale adaptive concrete beam with integrated fluidic actuators. *Civ. Eng. Des.* **2022**, *4*, 35–42. [CrossRef]

19. Wang, Y.; Senatore, G. Design of adaptive structures through energy minimization: Extension to tensegrity. *Struct. Multidiscipl. Optim.* **2021**, *64*, 1079–1110. [CrossRef]

20. Blandini, L.; Haase, W.; Weidner, S.; Böhm, M.; Burghardt, T.; Roth, D.; Sawodny, O.; Sobek, W. D1244: Design and Construction of the First Adaptive High-Rise Experimental Building. *Front. Built Environ.* **2022**, *8*, 4911. [CrossRef]

21. Wagner, J.L.; Gade, J.; Heidingsfeld, M.; Geiger, F.; von Scheven, M.; Böhm, M.; Bischoff, M.; Sawodny, O. On steady-state disturbance compensability for actuator placement in adaptive structures. *at—Automatisierungstechnik* **2018**, *66*, 591–603. [CrossRef]

22. Kelleter, C.; Burghardt, T.; Binz, H.; Blandini, L.; Sobek, W. Adaptive concrete beams equipped with integrated fluidic actuators. *Front. Built Environ.* **2020**, *6*, 107–119. [CrossRef]

23. Geiger, F.; Gade, J.; von Scheven, M.; Bischoff, M. A case study on design and optimization of adaptive civil structures. *Front. Built Environ.* **2020**, *6*, 94. [CrossRef]

24. Senatore, G.; Reksowardojo, A.P. Force and shape control strategies for minimum energy adaptive structures. *Front. Built Environ.* **2020**, *6*, 105. [CrossRef]

25. Steffen, S.; Zeller, A.; Böhm, M.; Sawodny, O.; Blandini, L.; Sobek, W. Actuation concepts for adaptive high-rise structures subjected to static wind loading. *Eng. Struct.* **2022**, *267*, 114670. [CrossRef]

26. Teuffel, P. Entwerfen Adaptiver Strukturen. Ph.D. Dissertation, Universität Stuttgart, Stuttgart, Germany, 2004.

27. Schnellenbach-Held, M.; Fakhouri, A.; Steiner, D.; Kühn, O. *Adaptive Spannbetonstruktur mit Lernfähigem Fuzzy-Regelungssystem: Bericht zum Forschungsprojekt 88.0107/2010*; Fachverlag NW: Bremen, Germany, 2014; ISBN 978-3-95606-084-7.

28. Bleicher, A. Aktive Schwingungskontrolle einer Spannbandbrücke mit pneumatischen Aktuatoren. *Bautechnik* **2012**, *89*, 89–101. [CrossRef]

29. Weilandt, A. Adaptivität bei Flächentragwerken. Ph.D. Dissertation, Universität Stuttgart, Stuttgart, Germany, 2008.

30. Heidenreich, C. Adaptivität von Freigeformten Flächentragwerken. Ph.D. Dissertation, Bauhaus-Universität Weimar, Weimar, Germany, 2016.

31. Kleine, T.; Wagner, J.L.; Böhm, M.; Sawodny, O. Optimal actuator placement and static load compensation for a class of distributed parameter systems. *at—Automatisierungstechnik* **2021**, *69*, 739–749. [CrossRef]

32. Marti, P. *Baustatik: Grundlagen, Stabtragwerke, Flächentragwerke, 2. Aufl.*; Ernst & Sohn: Berlin, Germany, 2014; ISBN 978-3-433-60436-3.

33. Pucher, A. *Einflußfelder Elastischer Platten = Influence Surfaces of Elastic Plates, 3. Aufl.*; Springer: Wien, Austria; Springer: New York, NY, USA, 1964.

34. Steffen, S.; Weidner, S.; Blandini, L.; Sobek, W. Using influence matrices as a design and analysis tool for adaptive truss and beam structures. *Front. Built Environ.* **2020**, *6*, 22–33. [CrossRef]

35. Steffen, S.; Blandini, L.; Sobek, W. Analysis of the inherent adaptivity of basic truss and beam modules by means of an extended method of influence matrices. *Eng. Struct.* **2022**, *266*, 114588. [CrossRef]

36. Kelleter, C.; Burghardt, T.; Binz, H.; Sobek, W. Actuation concepts for structural concrete elements under bending stress. In Proceedings of the 6th European Conference on Computational Mechanics (ECCM 6) and 7th European Conference on Computational Fluid Dynamics (ECFD 7), Glasgow, UK, 11–15 June 2018; Owen, R., Ed.; CIMNE: Barcelona, Spain, 2018. ISBN 978-84-947311-6-7.

37. Kelleter, C.; Sobek, W.; Burghardt, T.; Binz, H. Actuation of structural concrete elements under bending stress with integrated fluidic actuators. In Proceedings of the 7th International Conference on Structural Engineering, Mechanics and Computation (SEMC 7), Cape Town, South Africa, 2–4 September 2019; Zingoni, A., Ed.; CRC Press: Boca Raton, FL, USA, 2019; ISBN 978-1-138-38696-9.

38. Czichos, H. *Mechatronik: Grundlagen und Anwendungen technischer Systeme, 4., überarbeitete und erweiterte Auflage*; Springer: Wiesbaden, Germany, 2019; ISBN 9783658262945.

39. Isermann, R. *Mechatronische Systeme: Grundlagen*; Springer: Berlin/Heidelberg, Germany, 2008; ISBN 978-3-540-32336-5.

40. Werkle, H. *Finite Elements in Structural Analysis: Theoretical Concepts and Modeling Procedures in Statics and Dynamics of Structures*, 1st ed.; Springer International Publishing: Cham, Switzerland, 2021; ISBN 978-3-030-49840-5.

41. Geiser, A.; Oberbichler, T.; Sautter, K. Theory of Plates—Version 1.0.1 Nov. 2017. TUM Statik: München, Germany, 2017.

42. Felippa, C.A. Introduction to Finite Element Methods. In *Lecture Notes for the Course Introduction to Finite Element Methods*; Aerospace Engineering Sciences Department of the University of Colorado: Boulder, CO, USA, 2004.

43. Housner, G.W.; Bergman, L.A.; Caughey, T.K.; Chassiakos, A.G.; Claus, R.O.; Masri, S.F.; Skelton, R.E.; Soong, T.T.; Spencer, B.F.; Yao, J.T.P. Structural control: Past, present, and future. *J. Eng. Mech.* **1997**, *123*, 897–971. [CrossRef]

44. Hake, E.; Meskouris, K. *Statik der Flächentragwerke: Einführung mit Vielen Durchgerechneten Beispielen, 2. Aufl.*; Springer: Berlin/Heidelberg, Germany, 2007; ISBN 978-3-540-72624-1.

45. Penrose, R. A generalized inverse for matrices. *Math. Proc. Camb. Philos. Soc.* **1955**, *51*, 406–413. [CrossRef]

46. Czerny, F. Tafeln für Rechteckplatten. In *Beton-Kalender 1996, Teil I*; Eibl, J.W., Ed.; Ernst & Sohn Verlag: Berlin, Germany, 1996; pp. 277–330.